



HAL
open science

Reconstructing environments of collection sites from archaeological bivalve shells: Case study from oysters (Lyon, France)

Vincent Mouchi, Justine Briard, Stéphane Gaillot, Thierry Argant, Vianney Forest, Laurent Emmanuel

► To cite this version:

Vincent Mouchi, Justine Briard, Stéphane Gaillot, Thierry Argant, Vianney Forest, et al.. Reconstructing environments of collection sites from archaeological bivalve shells: Case study from oysters (Lyon, France). *Journal of Archaeological Science: Reports*, 2017, 21, pp.1225-1235. 10.1016/j.jasrep.2017.10.025 . hal-01628277

HAL Id: hal-01628277

<https://hal.sorbonne-universite.fr/hal-01628277v1>

Submitted on 3 Nov 2017

HAL is a multi-disciplinary open access archive for the deposit and dissemination of scientific research documents, whether they are published or not. The documents may come from teaching and research institutions in France or abroad, or from public or private research centers.

L'archive ouverte pluridisciplinaire **HAL**, est destinée au dépôt et à la diffusion de documents scientifiques de niveau recherche, publiés ou non, émanant des établissements d'enseignement et de recherche français ou étrangers, des laboratoires publics ou privés.

1 Reconstructing environments of collection sites from archaeological bivalve shells: case
2 study from oysters (Lyon, France)

3

4 Vincent Mouchi^{1*}, Justine Briard¹, Stéphane Gaillot², Thierry Argant^{3,4}, Vianney Forest⁵,
5 Laurent Emmanuel¹

6

7 ¹: Sorbonne Universités, UPMC-Univ. Paris 06, CNRS UMR 7193, Institut des Sciences de la
8 Terre de Paris (ISTeP), case 116, 4 pl. Jussieu, 75005 Paris, France

9 ²: Service archéologique de la ville de Lyon, 10 rue Neyret, FR-69001 Lyon

10 ³: Éveha, Études et valorisation archéologiques, agence Rhône-Alpes, 87 avenue des
11 Bruyères – 69150 Décines-Charpieu, France

12 ⁴: Laboratoire Archéométrie et Archéologie - UMR 5138

13 ⁵: INRAP-Méditerranée, TRACES-UMR5068-Toulouse, France

14 *: Corresponding author, current address: vmouchi@gmail.com

15

16

17 **Abstract**

18 The flat oyster, *Ostrea edulis*, was consumed as a luxury dish by the Romans in antiquity.

19 Numerous shells are found in archaeological sites in the Lyon region, Central France. This

20 area is located over 250 kilometres away from the nearest coastline (the Mediterranean Sea)

21 and little is known about the origin of these oysters prior to transport for consumption. The

22 chemistry of biogenic carbonates reflects that of the fluid they precipitate from at the time

23 of formation. Stable isotopes and Mg/Ca ratios in oyster shells have previously been used as

24 palaeoenvironmental proxies. As Mg/Ca ratio amplitude in bivalve shells has been reported

25 to differ according to local hydrologic settings, we suggest that geochemical differences
26 observed in each shell can be used to identify the type of environment (e.g. estuary, lagoon
27 or marine) from which the specimens originated.

28 In this study, we analyzed the elemental composition of six archaeological *O. edulis* shells of
29 unknown provenance, collected in the Lyon region dated from the 3rd century AD to the 5th
30 century AD. In addition, stable carbon and oxygen analyses from three of these specimens
31 were performed to reconstruct intra-annual fluctuations of seawater chemistry. Overall
32 results show a strong heterogeneity in values. One shell exhibits large fluctuations in $\delta^{13}\text{C}$
33 (from -2 to 1 ‰) and $\delta^{18}\text{O}$ (from -2 to 3 ‰), interpreted as evidence for an estuarine origin.
34 The Mg/Ca amplitude (from 5 to 35 mmol.mol⁻¹) also indicates proximity to a river outlet, as
35 such values were previously reported from modern estuarine oyster shells. Two other
36 specimens present a restricted amplitude in Mg/Ca values (from ~0 to 5 mmol.mol⁻¹), similar
37 to values measured in modern open marine locations. Four other specimens exhibited
38 intermediate Mg/Ca ratios and more restricted stable isotope composition ranges which
39 indicate that these specimens lived in waters with limited freshwater input.

40 The geochemical data from these shells support the hypothesis that fishermen of Antiquity
41 collected oysters from a variety of environments/locations. A clear identification of the living
42 localities of these specimens is still to be defined, as the present data cannot discriminate
43 whether these shells originated from the Mediterranean Sea or the Atlantic Ocean coastline.

44

45

46 **Introduction**

47 The flat oyster, *Ostrea edulis*, was consumed as a luxury dish by the Romans during
48 Antiquity. As a result, numerous shells are commonly found in archaeological sites of rich

49 dwelling places in the Lyon region, Central France. As this city is 250 km away from the
50 nearest coastline (Mediterranean Sea), these specimens were transported for consumption
51 and little is known on their locality of origin during the Roman Empire. Bardot-Cambot
52 (2014) reconstructed a map of commercial routes from this period, and suggested that most
53 molluscs in Lyon originated from the Mediterranean Sea. Though still debated, oyster
54 farming on the French Mediterranean coastline is thought to have started during the 19th
55 century AD (Bardot-Combot and Forest, 2013; Faget, 2007). Using an archaeozoological
56 approach applied to Roman shells supplemented by written sources analysis, Bardot-Combot
57 and Forest (2013) suggested that Romans did not perform aquaculture *per se* and probably
58 collected wild oysters. Hence, the exact localities and living environments of fished oysters
59 remain unknown.

60 The environmental record of geochemical fluctuations in oyster shells represents a
61 promising proxy for palaeoenvironment reconstructions. Oysters appeared over 200 million
62 years ago and their thick calcite shells are generally preserved with regards to diagenesis
63 (Stenzel, 1971). Moreover, they offer sufficiently large structures for high-resolution
64 sampling to study intra-annual (e.g. seasonal) fluctuations for several consecutive years of
65 growth (Kirby et al., 1998; Lartaud et al., 2010a; Surge and Lohmann, 2008).

66 The chemistry of biogenic carbonates reflects that of the fluid it precipitates from at the time
67 of formation (Epstein et al., 1951, 1953; McCrea, 1950). Bivalve shells present incremental
68 growth that preserve older parts, which allows for a continuous record of the evolution of
69 seawater composition during the organism's lifespan. Such mollusc shells have been used in
70 Earth Sciences since the middle of the 20th century (Urey et al., 1951) for reconstructing
71 physicochemical parameters of seawater. In particular, seasonal temperature
72 reconstructions of seawater have been proposed for geological timescales (i.e., several

73 hundred million years ago) using fossils (Anderson and Arthur, 1983; Craig, 1965; Epstein et
74 al., 1951, 1953). These estimates from shell analysis are based on modern breeding in
75 natural sites or laboratory experiments under controlled conditions that lead to the
76 formulation of mathematical equations linking shell geochemistry and physicochemical
77 parameters of seawater (i.e., temperature, salinity, pH). These models can subsequently be
78 utilized to determine past environmental settings.

79 Stable carbon isotopes ($\delta^{13}\text{C}$) in mollusc shells have been reported to depend on the
80 combination of the influence of both dissolved inorganic carbon (DIC) and organic carbon
81 sources from food consumption (Lartaud et al., 2010b; McConnaughey and Gillikin, 2008). It
82 has been demonstrated that $\delta^{13}\text{C}$ signals from oyster soft tissues (Gaudron et al., 2016) and
83 shells (Walther and Rowley, 2013) differ from purely marine to estuarine environments due
84 to distinct food sources. In particular, shell $\delta^{13}\text{C}$ can be used jointly with stable oxygen
85 isotope measurements to indicate flooding events (Walther and Rowley, 2013).

86 Several temperature proxies are commonly used on mollusc shells such as stable oxygen
87 isotope $^{18}\text{O}/^{16}\text{O}$ ratios ($\delta^{18}\text{O}$; Bougeois et al., 2014, 2016; Duprey et al., 2015; Epstein et al.,
88 1951, 1953; Klein et al., 1996; Lartaud et al., 2010c; Surge and Lohmann, 2008; Surge et al.,
89 2001; Vander Putten et al., 2000). Some uncertainties exist since calcium carbonate of the
90 shells $\delta^{18}\text{O}$ ($\delta^{18}\text{O}_\text{c}$) is a function of temperature and seawater $\delta^{18}\text{O}$ ($\delta^{18}\text{O}_\text{w}$). This last
91 parameter co-varies with salinity, which is often not properly constrained in the past
92 (Rohling, 2000). A variety of calibrations of $\delta^{18}\text{O}_\text{w}$ from salinity have been published based on
93 different modern marine settings (e.g., Epstein and Mayeda, 1953; Pierre, 1999; Voelker et
94 al., 2015), and a specific model is chosen according to the studied locality. Classically,
95 palaeosalinities are estimated by studying the ecology of the fauna associated with the
96 studied material or by taking modern values in similar settings. Temperatures are

97 reconstructed from these estimations of $\delta^{18}\text{O}_w$ and the measured $\delta^{18}\text{O}_c$ (McCrea, 1950).
98 Multiple models also exist for this relationship according to the mineralogy and the taxon.
99 For calcitic mollusc shells, such as oyster shells, the calibration provided by Anderson and
100 Arthur (1983) is relevant and widely utilized (Equation 1).
101 Equation 1: $T = 16 - 4.14 (\delta^{18}\text{O}_c - \delta^{18}\text{O}_w) + 0.13 (\delta^{18}\text{O}_c - \delta^{18}\text{O}_w)^2$ (Anderson and Arthur,
102 1983)
103 Strontium to calcium and magnesium to calcium ratios have also been exploited as
104 temperature proxies in biogenic carbonates (Bougeois et al., 2014, 2016; Freitas et al., 2008,
105 2012; Klein et al., 1996; Lazareth et al., 2003; Mouchi et al., 2013; Surge and Lohmann, 2008;
106 Ullmann et al., 2013; Vander Putten et al., 2000; Wanamaker et al., 2008). These Me/Ca
107 ratios in carbonates are also commonly considered to fluctuate according to several factors.
108 Mineralogy has an influence and each locality used for model definition has different
109 environmental settings which are reflected in the shell geochemistry.
110 Although these proxies were proven useless in some bivalve species such as clams (Carré et
111 al., 2006; Gillikin et al., 2005; Poulain et al., 2005; Surge and Walker, 2006) or scallops
112 (Lorrain et al., 2005), temperature seems to be the main factor causing fluctuations within a
113 specimen for mussels and oysters (Freitas et al., 2008; Klein et al., 1996; Mouchi et al., 2013;
114 Surge and Lohmann, 2008; Tynan et al., *in press*; Vander Putten et al., 2000). Still, some vital
115 effects (compositional shifts from seawater composition and physicochemical parameter
116 response) may induce at least a certain amount of geochemical variability (Bougeois et al.,
117 2014, 2016; Mouchi et al., 2013; Saenger and Wang, 2014; Schöne and Gillikin, 2013).
118 Magnesium incorporation in single oyster shells presents different calculated
119 thermodependance equations when considering calcification that occurred from autumn to
120 winter (decreasing temperatures) compared to the period from spring to summer

121 (increasing temperatures), probably due to different metabolic response (see Fig. 6 in
122 Mouchi et al., 2013). This metabolic impact prevents the effective use of Mg/Ca for
123 temperature reconstructions for spring and autumn, restricting estimations from this proxy
124 to thermal amplitude between winter and summer. Mouchi et al. (2013) also reported that
125 high-frequency and large amplitude fluctuations in shell Mg/Ca correspond to successive
126 lunar cycles not related to temperature variations.

127 Finally, for the marine and brackish mussel genus *Mytilus*, a clear locality-specificity was
128 noted in Mg incorporation (Freitas et al., 2008; Klein et al., 1996; Vander Putten et al., 2000;
129 Wanamaker et al., 2008). The same observation was made for the *Saccostrea glomerata*
130 oyster species (Tynan et al., *in press*). A model must therefore be carefully chosen to avoid
131 incorrect interpretations.

132 In this study, using isotopic and elemental analyses of the shells, we gather physicochemical
133 evidence to characterize the historically important fishing areas. As geomorphology of the
134 Mediterranean coastline presented strong heterogeneity in Antiquity (Carozza et al., 2010;
135 Dubar, 2003; Raynal et al., 2010; Rescanières, 2002; Rey et al., 2009), these various settings
136 should be reflected in the geochemistry of oyster shell specimens. In particular, using the
137 locality-specificity of Mg/Ca in oyster shells, we attempt to define whether fishermen had
138 clustered sources of oysters or if they collected from a broader variety of environments.

139 **Materials and Methods**

140 Archaeological sites

141 The oyster specimens (*Ostrea edulis*) used in this study were collected from archaeological
142 sites in Lyon, France. The first site, referred to as Antiquaille (Hofmann, *in prep*), corresponds
143 to an abandoned residential area located on the Fourvière hill, at the heart of the *Lugdunum*
144 primitive colony. Eleven oyster specimens were selected from the community found on this

145 site. The stratigraphic unit from which those shells were collected was dated to the 2nd or 3rd
146 century AD by ceramics.

147 A second collection site corresponds to a filling pit dated to the 5th century AD on the 16 rue
148 Bourgelat site (Bertand, 2011). This large pit (3.70 by 5.5 m) included small items (fauna
149 remains, ceramics) and large quantities of broken parts from furnaces and dwelling places.

150 The quality of these broken parts indicates the demolition of wealthy residences. The top of
151 this pit is in direct contact with the modern age levels. A total of 51 oyster shells were
152 recovered from this site as well as some Bourgogne snails (*Helix pomatia*) shells. Twelve
153 oyster specimens were selected from this site.

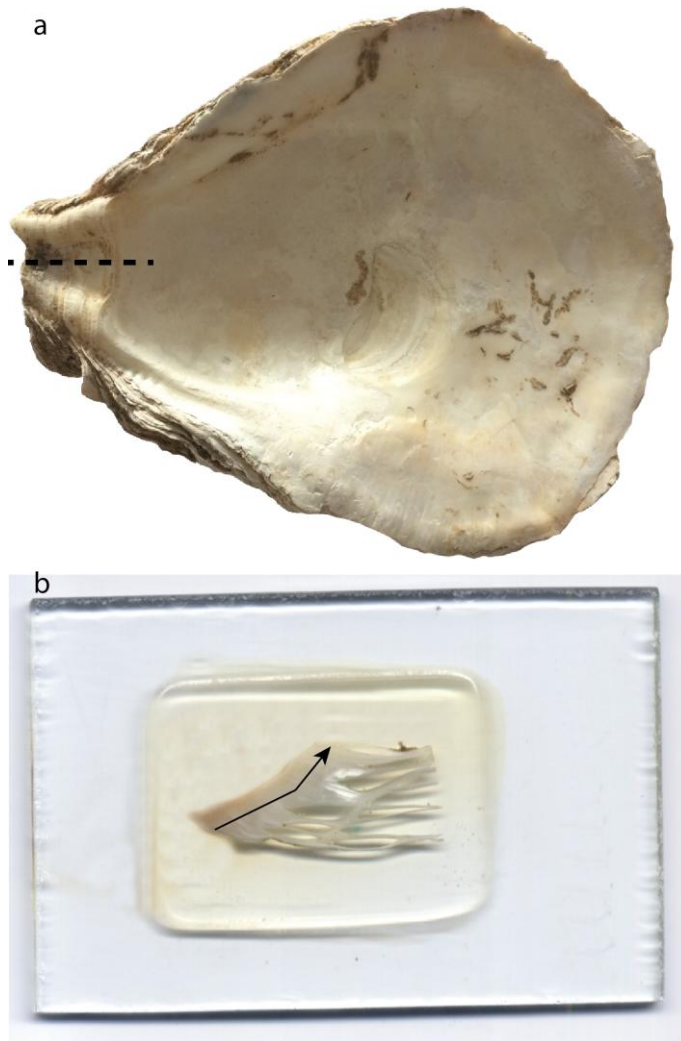
154 Finally, three shells were selected from the 8-14 rue Gadagne site, in the Old Lyon district.
155 This site is located on the east side of the Saône River at the base of the Fourvière hill. It was
156 built from 50-70 BC, prior to *Lugdunum* foundation. During the Gallo-Roman age, a large
157 building was occupied between the 3rd and the 4th centuries AD.

158 All specimens are considered to have been consumed by a high social level community and
159 must have travelled some considerable distance from a coastline. Although most specimens
160 probably originated from the Mediterranean Sea, bivalve shells from species endemic to the
161 Atlantic coastline have been discovered on site (Bardot-Cambot, 2014). The exact origin of
162 the oysters consumed in Lyon during Antiquity is therefore still unknown.

163 Oyster shells

164 Specimens presenting no visible perforation in the umbo region by lithophagous fauna were
165 manually cleaned from potential epibionts attached on the shell surface using deionized
166 water. Ultrasonic baths were not utilized due to the fragile aspect of our specimens. The
167 umbo region of the left valve was mounted in resin and cut from the rest of the shell using a
168 Buehler Isomet Low Speed Saw (Huntsman Araldite 2020) in order to prevent the fine

169 lamellae inside the umbo from breaking during preparation. Polished thick sections (200-500
170 μm thick) were cut along the maximum growth axis to expose the inner part of the umbo
171 (Fig. 1). This process allows access to a complete and continuous accretionary growth record
172 on a spatially-restricted area (Bougeois et al., 2014, 2016; Kirby et al., 1998; Langlet et al.,
173 2006; Lartaud et al., 2010a; Mouchi et al., 2013; Richardson et al., 1993).



174

175 Figure 1: Oyster sample preparation. a: Left valve of oyster shell showing location and
176 orientation of cut from the umbo. b: Thin section from the cut located on a. The arrow
177 indicates the direction of growth and location of Mg/Ca transect measurements.

178

179 Seasonal calibration using cathodoluminescence

180 The umbo region of each oyster shell was observed under cathodoluminescence (CL) using
181 the principles described in Langlet et al. (2006) and Lartaud et al. (2010c). Natural
182 luminescence is emitted in response to electronic bombardment due to the presence of
183 activators (mainly Mn) within the crystal lattice. The intensity of luminescence (IL) is mainly
184 related to the proportion of Mn^{2+} (de Rafé́lis et al., 2000). It has been observed that Mn^{2+}
185 incorporation in the shell is increased during summer months compared to the winter
186 (Langlet et al., 2006; Lartaud et al., 2010c). This is due to enhanced phytoplankton
187 consumption in summer (with more frequent blooms), as phytoplankton species can
188 incorporate up to 4 orders of magnitude of Mn compared to surrounding waters (Sunda and
189 Huntsman, 1985). This cyclic annual Mn concentration pattern has been used as a temporal
190 calibration of mineral accretion in the umbo of fossil oyster shells (Bougeois et al., 2014,
191 2016; Lartaud et al., 2006). CL also allows to attest the pristine state of calcium carbonate
192 structures.

193 CL observations were undertaken with a Cathodyne-OPEA cold cathode at 15-20 kV and 200-
194 400 $\mu A \cdot mm^{-2}$, with a pressure of 0.05 Torr. No diagenetic overprint was noted on any of the
195 26 specimens. Assembly of colour pictures of the observation of each specimen was
196 converted to grey-scale and line transects following shell growth in the foliated area were
197 chosen for analysis with the NIH-ImageJ software (v. 1.50i). These transects of grey intensity
198 variations were then used to locate areas of bright luminescence (i.e. are synchronous to
199 summer periods) and dull luminescence (associated to winter periods). Six specimens from
200 the initial 26 were selected for further analyses according to the quality of this temporal
201 calibration: four specimens from stratigraphical units dated to the 2nd or 3rd century AD in
202 Site 1 (US547-1, US654-1, US654-3 and US915-1), one specimen from a stratigraphical unit
203 dated to the 5th century AD in Site 2 (US46-2) and a final specimen from a stratigraphical unit

204 dated to the 4th century AD in site 3 (US118-3).

205 Geochemical analyses

206 *Mg/Ca ratios*

207 The six selected shells were carbon coated and analyzed by electron probe microanalysis
208 (EPMA) at the Camparis service of IStEP, UPMC, Paris. A CAMECA SX *Five* was used,
209 operating at 25 kV potential with a 130 nA current and 25 µm defocused beam diameter, as
210 used by Mouchi et al. (2013). Detection limits for the measured elements were 100 ppm for
211 Ca and 60 ppm for Mg. A diopside crystal was used as an internal standard for both
212 elements. According to the size of the specimens, successive interconnected transects (to
213 accommodate for the curvature of the umbo; Fig. 1b) were performed along the foliated
214 area of the umbo presenting no obvious physical alteration to obtain several continuous
215 millimeters of elemental measurements per specimen. With the chosen sampling resolution,
216 we obtained between 244 and 497 regularly spaced (25 µm) measurements per shell.
217 High-frequency fluctuations (which do not reflect physicochemical parameters of seawater;
218 Mouchi et al., 2013) were removed by performing a moving average on 15 points on all data
219 series.

220 *Stable oxygen and carbon isotope ratios*

221 Stable carbon and oxygen isotopic analyses were performed on three of the specimens
222 following umbo growth. For each sample, 40 µg of powder were collected from thick
223 sections using a micromill at the Muséum National d'Histoire Naturelle, Paris. Drilling was
224 operated to extract carbonate powder from separated curved transects over 1-2 mm long
225 (depending on the available space of foliated calcite) and 250 µm depth for each sample.
226 Seasonal calibration from CL was used to define a resolution allowing multiple samples per
227 season when possible for consistency over several successive years of accumulation. We

228 collected 12 samples for isotope analysis from specimen US547-1 (2 samples were rejected
229 due to lack of material), 23 samples from specimen US46-2 (no rejection) and 17 samples
230 from specimen US654-1 (1 sample rejected due to lack of material). Carbon dioxide was
231 extracted on carbonate powder using a Kiel IV carbonate device after dissolution in anhydric
232 orthophosphoric acid at 70°C (McCrea, 1950) and analyses were performed on a DELTA V
233 isotope ratio mass spectrometer at the Université Pierre et Marie Curie (Paris, France).
234 Isotope values are reported in delta notation relative to Vienna Peedee Belemnite. Repeated
235 analyses of a marble working standard (calibrated against the international standard NBS-19)
236 indicate an accuracy and precision of 0.1‰ (1 σ).
237 For temperature estimations, the model of Anderson and Arthur (1983; Equation 1) was
238 used for thermodependance of shell $\delta^{18}\text{O}$. The model of Pierre (1999), defined from current
239 values of the Mediterranean Sea, was used for estimating $\delta^{18}\text{O}_w$ (Equation 2). As a
240 comparative model for $\delta^{18}\text{O}_w$, we used the model of Lartaud (2007) which was established
241 from different locations from the French Atlantic and the English Channel coastline
242 (Equation 3).

243 Equation 2: $\delta^{18}\text{O}_w = 0.27 * S - 8.9$ Pierre (1999)

244 Equation 3: $\delta^{18}\text{O}_w = 0.22 * S - 7.3$ Lartaud (2007)

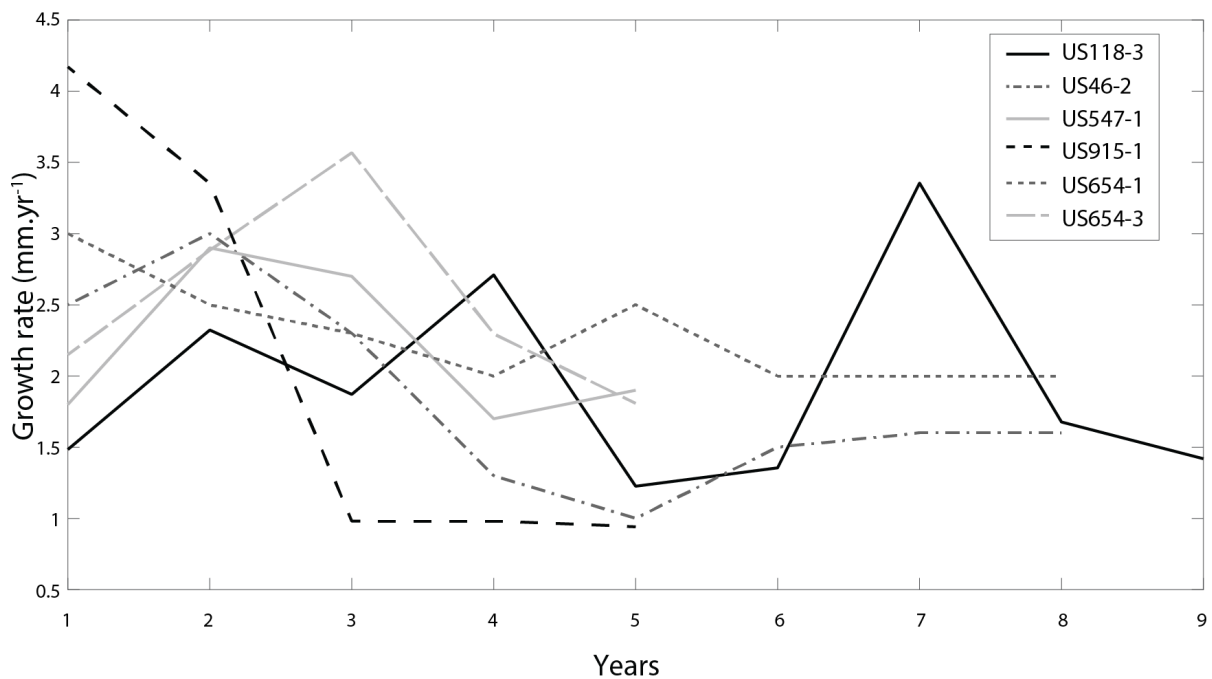
245

246 **Results**

247 Growth rates

248 According to the studied specimens, different behaviors are observed concerning the growth
249 rates (Fig. 2) when using cathodoluminescence as temporal calibration (high luminescence
250 corresponds to summer periods; low luminescence to winter periods). The specimens US46-
251 2, US654-1, US654-3, US547-1 and US915-1 present a decreasing growth rate over time in

252 accordance to the classic growth model of von Bertalanffy. US915-1 presents very high
 253 growth rates during the juvenile stage ($> 4 \text{ mm.yr}^{-1}$), whereas shell growth rates from all
 254 other specimens range between 1.8 and 3 mm.yr^{-1} . The specimen US118-3 displays a
 255 particular behavior with a relatively low juvenile growth rate (1.5 mm.yr^{-1}) and an increase of
 256 calcification rate during its fourth and seventh year (based on cathodoluminescence
 257 temporal calibration).



258
 259 Figure 2: Reconstructed growth rates from all specimens based on cathodoluminescence
 260 temporal calibration (Langlet et al., 2006; Lartaud et al., 2010c).

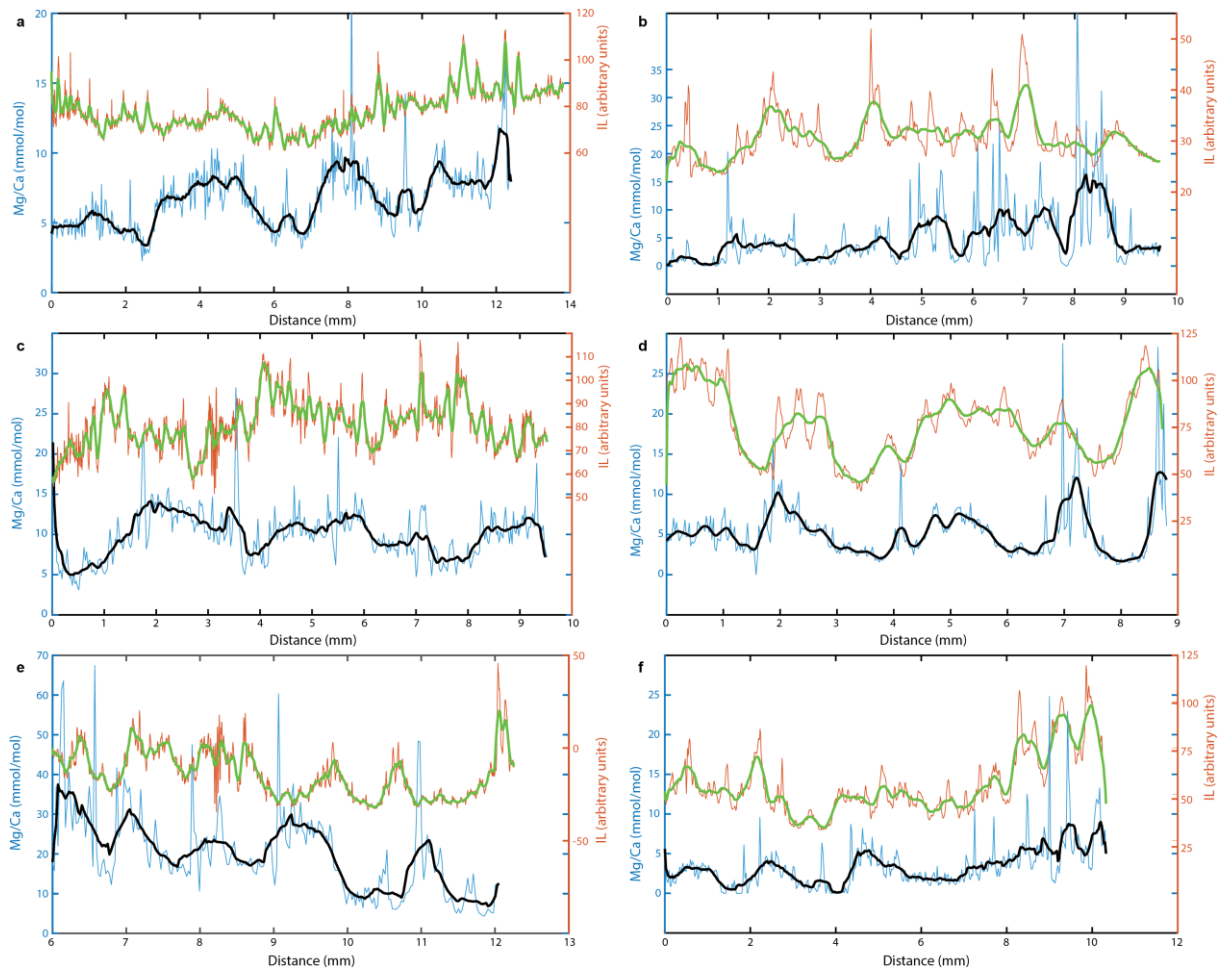
261
 262 Mg/Ca variations

263 All specimens exhibit Mg/Ca fluctuations (Fig. 3). Several groups of specimens can be
 264 differentiated from ranges of values of low frequency fluctuations (see smoothed data on
 265 Fig. 3). Specimens US547-1 (Fig. 3a) and US654-3 (Fig. 3d) present a range of values from
 266 approximately 3 to approximately 10 mmol.mol^{-1} , with mean values of 6.67 ± 2.23 and 5.21
 267 $\pm 3.37 \text{ mmol.mol}^{-1}$ for US547-1 and US654-3, respectively. A second group is defined by

268 specimens US118-3 (Fig. 3b) and US915-1 (Fig. 3f) with lower values, generally ranging from
269 approximately 1 to 5 mmol.mol⁻¹, although specimen US118-3 presents increased amplitude
270 with ontogeny. Mean values are 4.90 ± 5.58 and 3.32 ± 2.82 mmol.mol⁻¹ for US118-3 and
271 US915-1, respectively. Specimen US654-1 (Fig. 3c) exhibits values ranging from 7 to 12
272 mmol.mol⁻¹ approximately (9.99 ± 3.20 mmol.mol⁻¹). Finally, specimen US46-2 (Fig. 3e) has
273 the highest values of the dataset, ranging from 5 to 35 mmol.mol⁻¹ with a mean value of
274 19.74 ± 10.70 mmol.mol⁻¹. A positive ontogenic trend is visible for specimen US547-1 (Fig.
275 3a) and a negative trend is visible for specimen U46-2 (Fig. 3e).

276 When compared to luminescence intensity (IL), specimens US118-3 (Fig. 3b), US654-3 (Fig.
277 3d) and US915-1 (Fig. 3f) present a fair graphic correlation between cathodoluminescence
278 signal and Mg/Ca for the entire studied transects. Graphic correlation for specimen US547-1
279 (Fig. 3a) can be validated until 8 mm from the start of the hinge (Fig. 3a). Specimens US547-1
280 and US46-2 exhibit partial graphic correlation only. Specimen US46-2 presents a positive
281 graphic correlation at first from 6 to 8.5 mm on the transect, while the rest of the measured
282 line presents Mg/Ca values that do not reflect any resemblance to the IL signal (Fig. 3e).

283 Relation between these two signals is more complex for specimen US654-1 which seem to
284 present a partial anti-correlation from 1 to 4 mm and from 5.5 to 8.5 mm (Fig. 3b).



285

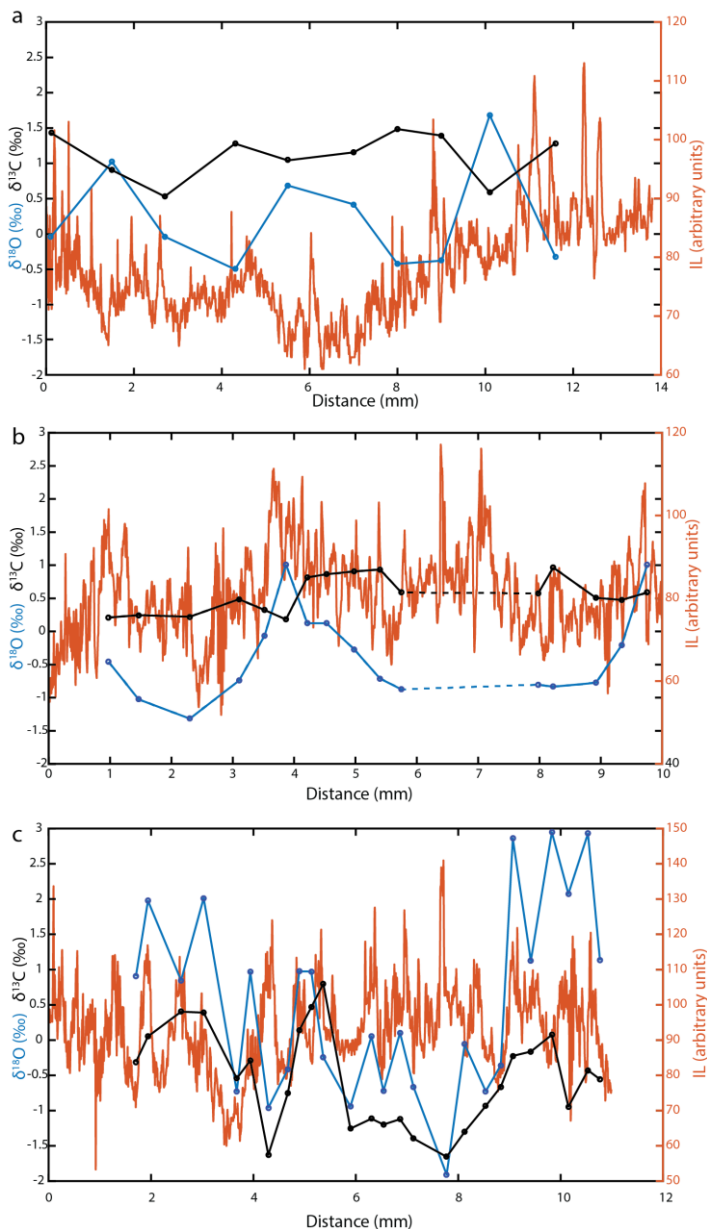
286 Figure 3: CL intensity of luminescence (IL; in arbitrary units) and Mg/Ca ratio along the
 287 measured transects of all six specimens. The abscissa represents the distance from the start
 288 of the hinge, following growth. Moving average smoothing (15 points for Mg/Ca and 25
 289 points for IL) are also indicated in black (Mg/Ca) and green (IL) for clarity. Note the scales for
 290 Mg/Ca ratios. a: US547-1. b: US118-3. c: US654-1. d: US654-3. e: US46-2 (adult part only). f:
 291 US915-1.

292

293 Isotope ratios

294 The $\delta^{18}\text{O}$ values range from -0.50 to 1.68 ‰ (mean: 0.21 ± 0.73 ‰) for specimen US547-1,
 295 from -1.32 to 1.01 ‰ (mean: -0.36 ± 0.67 ‰) for US654-1 and from -1.91 to 2.95 ‰ (mean:
 296 0.54 ± 1.34 ‰) for US46-2 (Fig. 4). The $\delta^{13}\text{C}$ values range from 0.53 to 1.48 ‰ (mean: $1.11 \pm$

297 0.34 ‰), from 0.18 to 0.96 ‰ (mean: 0.56 ± 0.28 ‰) and from -1.66 to 0.80 ‰ (mean: -0.54
 298 ± 0.69 ‰) for US547-1, US654-1 and US46-2, respectively.
 299 Variations of IL generally present opposed fluctuations with $\delta^{18}\text{O}$ for specimen US547-1. On
 300 the contrary, specimen US654-1 shows synchronous fluctuations of IL and $\delta^{18}\text{O}$. Specimen
 301 US46-2 presents strong fluctuations with little relation to IL variations.



302
 303 Figure 4: Isotopic ratios (axis on the left-hand side) from all three shells in relation to CL
 304 intensity of luminescence (IL). a: US547-1. b: US654-1. The dashed transect marks a
 305 damaged portion of the shell that was not sampled. c: US46-2.

306

307 **Discussion**

308 Reconstructing seasonal evolution of seawater chemistry from stable isotope analyses

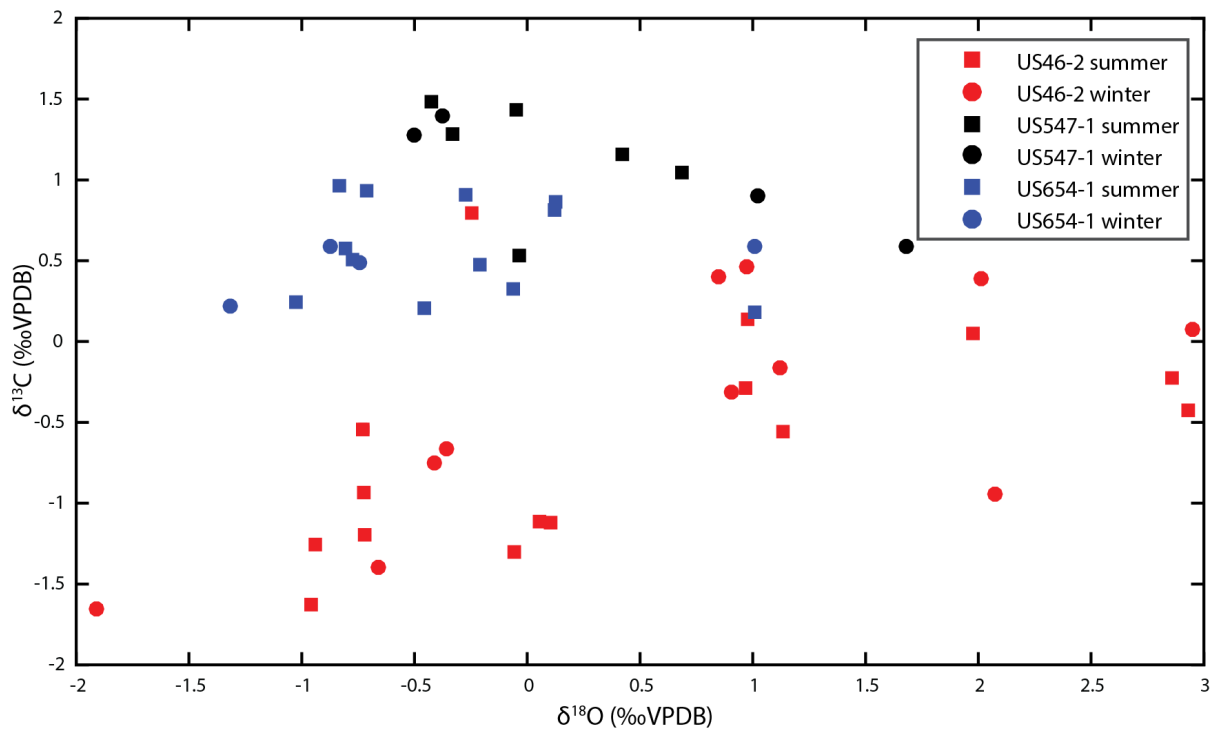
309 When evaluating the results for $\delta^{13}\text{C}$ and $\delta^{18}\text{O}$, additional information can be inferred about
310 the temporal dynamic change of the surrounding waters along the organism's lifespan.

311 Figure 5 presents the seasonal record of isotopic composition of the studied shells. Upon
312 initial observation there is no obvious seasonal difference between $\delta^{13}\text{C}$ and $\delta^{18}\text{O}$ for each
313 specimen (Fig. 5). Secondly, specimens US547-1 and US654-1 are relatively restricted in
314 amplitude for $\delta^{13}\text{C}$, with US547-1 values more enriched than those of US654-1. Finally, US46-
315 2 presents larger amplitudes in both $\delta^{13}\text{C}$ and $\delta^{18}\text{O}$ and $\delta^{13}\text{C}$ values are generally depleted
316 compared to the other specimens. In oyster shells, $\delta^{13}\text{C}$ values generally reflect fluctuations
317 in dissolved inorganic carbon (DIC) and/or organic carbon from diet (phytoplankton) whose
318 interactions, challenging to constrain, complicate the interpretation as an environmental
319 proxy (Emery et al., 2016; Klein et al., 1996; Lartaud et al., 2010b; Surge and Lohmann, 2008;
320 Surge et al., 2003). Still, this large amplitude indicates that specimen US46-2 was living in a
321 less stable environment than both other specimens in terms of food supply and salinity.

322 The initial part of the US46-2 shell presents relatively enriched values for both isotope ratios
323 (Fig. 4c). Two features are noted for this part of the sequence involving a sudden decrease in
324 both $\delta^{13}\text{C}$ and $\delta^{18}\text{O}$. A drop in $\delta^{18}\text{O}$ can be interpreted as both an increase in temperature
325 and a drop in salinity. If we consider that this specimen originates from the French
326 Mediterranean coastline, the main river reaching this area is the Rhone River, whose flow is
327 controlled by the melting of the Alps glaciers. Thus, an increase in temperatures recorded in
328 the Mediterranean Sea can also be synchronously happening in the Alps and cause stronger
329 melting, inducing a more pronounced flow of the Rhone River. This larger amount of

330 freshwater, when reaching the shore, would subsequently be responsible for a decrease of
331 salinity, as observed in the present data. However, other possibilities to provide freshwater
332 exist, such as important floods during high-intensity rainfall events. Indeed, it has been
333 reported that strong variations in $\delta^{13}\text{C}$ and $\delta^{18}\text{O}$ in oyster shells can be linked to flooding
334 events (Walther and Rowley, 2013). Such events can also be proposed as a cause for a non-
335 seasonal Mn incorporation (and hence CL signal) as nutrient input would vary and induce
336 episodic Mn-rich phytoplankton blooms. Such an interpretation would explain the
337 complexity of the CL signal from this specimen (Fig. 4c) compared to the others.
338 The synchronous decrease in $\delta^{13}\text{C}$ can also be explained by the same type of event, as cold
339 freshwater reaching the shore from melting glaciers would contain substantial
340 concentrations of nutrients. These nutrients would induce phytoplankton development,
341 reducing the DIC $\delta^{13}\text{C}$ as organic matter incorporates more ^{12}C , but would provide a
342 substantial food source for the oysters, which would in turn enrich their shells in light
343 carbon.

344 For the rest of the shell, when following growth, several clusters of $\delta^{13}\text{C}$ and $\delta^{18}\text{O}$ are
345 recorded. It seems that local seawater conditions lingered at a certain steady-state before
346 being strongly and suddenly changed to a new equilibrium for another few years. Contrary
347 to the other specimens that demonstrate more stable conditions, it seems here that US46-2
348 is native to a dynamic location.



349

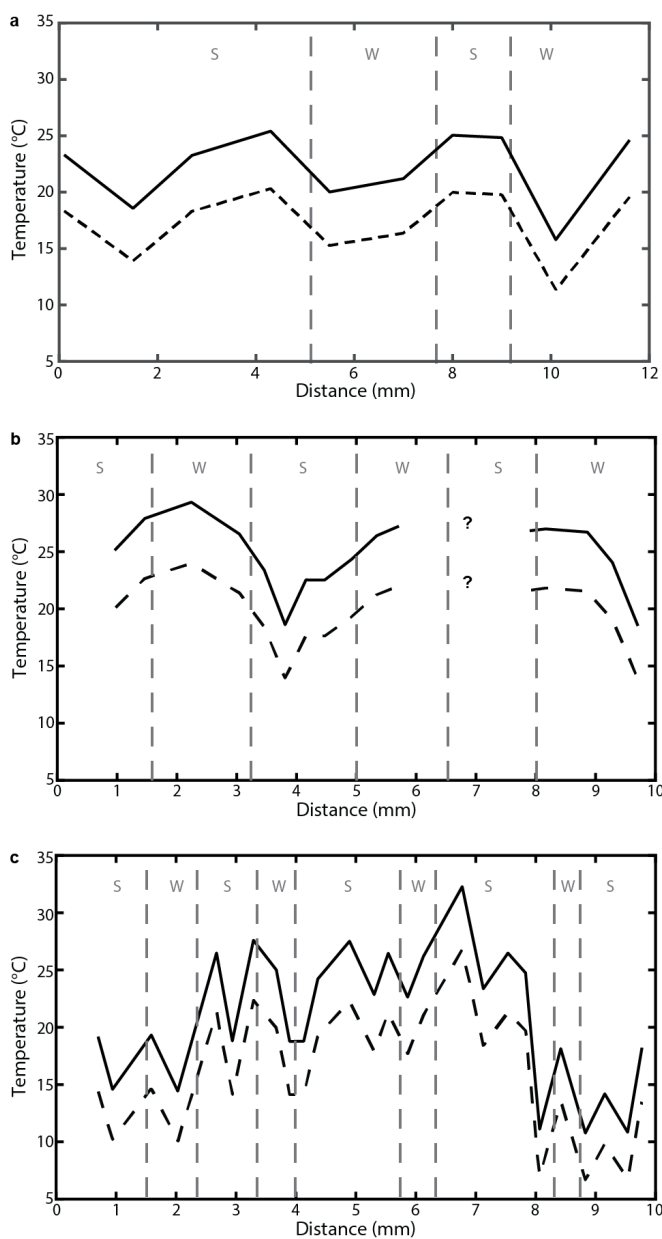
350 Figure 5: Isotopic composition of oyster shells. Samples from winter and summer periods of
 351 calcification (from interpretation of CL signal) are discriminated. US547-1 (in black, 10
 352 samples), US654-1 (in blue, 16 samples) and US46-2 (in red, 26 samples) show 2 different
 353 signals. Specimens US547-1 and US654-1 present a restricted amplitude in O and C isotopic
 354 composition, while specimen US46-2 exhibits a large amplitude of values for both isotopic
 355 ratios.

356

357 Temperature reconstruction using estimated $\delta^{18}\text{O}_w$

358 Oxygen isotope ratios were converted to temperatures using the equation of Anderson and
 359 Arthur (1983) based on calcitic molluscs (Equation 1). As an estimation of $\delta^{18}\text{O}_w$ – required
 360 for the temperature calculations – we used the equations of Pierre (1999; Equation 2) and
 361 Lartaud (2007; Equation 3), defined from the Mediterranean Sea and the French Atlantic
 362 coastline, respectively. To do this, we used a constant modern mean salinity value of 35.5 ‰
 363 for the Atlantic area model and 39.0 ‰ for the Mediterranean area model. The

364 corresponding calculated $\delta^{18}\text{O}_w$ values from Equations 2 and 3 are 1.63 ‰ and 0.51 ‰ for
365 the Mediterranean Sea and the North-East Atlantic, respectively. Resulting calculations are
366 shown on Figure 6. As growth rates of oyster shells are known to be reduced in winter
367 months (Lartaud et al., 2010c) and since our sampling resolution is spatially constant
368 between consecutive samples, winter values are likely to be overestimated (i.e., samples
369 from winter periods will probably contain parts from previous autumn and/or subsequent
370 spring, inducing an elevated mean value).



371

372 Figure 6: Temperature reconstruction from $\delta^{18}\text{O}$ for two hypothetical origins of the oyster

373 shells: Mediterranean Sea (solid line) and French Atlantic coast (dashed line). Values of $\delta^{18}\text{O}_w$
374 used for calculations using the model of Anderson and Arthur (1983) are 1.63 ‰
375 (considering a constant salinity of 39 ‰ and using the model of Pierre, 1999; Equation 2) and
376 0.51 ‰ (considering a constant salinity of 35.5 ‰ and using the model of Lartaud, 2007;
377 Equation 3) for the Mediterranean Sea and the North-East Atlantic, respectively. Limits of
378 winter (W) and summer (S) seasons, based on CL model (Langlet et al., 2006), are located by
379 dashed vertical grey lines. a: US547-1. b: US654-1. The missing transect (underlined by '?'
380 signs) corresponds to a damaged part of the shell that was not sampled. c: US46-2.

381

382 Temperatures reconstructed using this estimated constant $\delta^{18}\text{O}_w$ show generally
383 synchronous fluctuations for specimen US547-1 compared to the seasons interpreted from
384 CL signal (Fig. 6a). Temperature values range from 11.3 to 20.3 °C for the Atlantic hypothesis
385 and from 15.8 to 25.4 °C for the Mediterranean Sea hypothesis, though most variations
386 occur over a modelled 6 to 7 °C interval for the entire section, which is lower than the values
387 currently measured on the French coasts (generally 16 °C amplitude for the Mediterranean
388 Sea, from 11 to 27 °C, and approximately 12 °C amplitude for the Atlantic, from 8 to 20 °C;
389 <http://www.meteociel.fr/accueil/sst.php>). The calculated summer temperature values for
390 the Mediterranean Sea origin hypothesis are in accordance with Luterbacher et al. (2016),
391 who indicated for this period that mean summer temperatures for the studied time period
392 were approximately 2.5°C lower than those from present day.

393 For specimen US654-1, reconstructed temperatures range from 14 to 24 °C for the Atlantic
394 hypothesis, corresponding to a modelled temperature amplitude of 10 °C (Fig. 6b). For the
395 Mediterranean origin hypothesis, reconstructed temperatures range from 18.6 to 29.3 °C.

396 The age model from CL appears here to be contrary to the calculated temperatures. The

397 second winter and third summer indicated by the CL fluctuations has however no
398 corresponding isotope samples to check for this discrepancy. Still, subsequent samples,
399 which would correspond to a winter period, present high temperatures and slowly
400 decreasing at the end of this winter period, which is consistent with previous parts of this
401 shell.

402 Specimen US46-2 presents temperatures ranging from 6.7 to 26.7 °C for the Atlantic
403 hypothesis and from 10.8 to 32.3 °C considering a Mediterranean origin, corresponding to a
404 thermal contrast on the extrema of over 20 °C (Fig. 6c). However, a positive trend is visible
405 from the start to 7.5 mm before a strong drop in values. When comparing to local minima
406 and maxima, the contrast rarely exceeds 10 °C. High and low temperature values do not
407 reflect CL seasons, which tends to indicate that this specimen lived in a less stable
408 environment than specimens US547-1 and US654-1. In this specimen, salinity must have
409 varied throughout the organism's lifespan, and probably from one season to the next (see
410 Fig. 4), suggesting some freshwater influence in substantial proportions to significantly
411 change the $\delta^{18}\text{O}_w$. Indeed, seasonal or monthly fluctuations in $\delta^{18}\text{O}_w$ have been reported to
412 induce errors of $\pm 3^\circ\text{C}$ in estimations of sea surface temperatures compared to a mean
413 annual value, even without important freshwater influence (e.g. Prendergast et al., 2013).
414 For all specimens, none of the hypotheses (Atlantic Ocean or a Mediterranean Sea origin for
415 the oyster shells) can be ruled out from the reconstructed temperatures. As stable isotope
416 values cannot efficiently discriminate the living environment, other methods need to be
417 investigated.

418 Environmental interpretation and collection sites in ancient times

419 In view of the stable isotope data discussed above, we note an influence of the level of
420 freshwater input from rivers on Mg/Ca in addition to temperature. However, salinity was

421 reported to have no influence in Mg/Ca in mussel (Vander Putten et al., 2000) and oyster
422 shells (Mouchi et al., 2013; Surge and Lohmann, 2008; Tynan et al., *in press*) and Mg
423 concentrations in seawater is not linked to Mg incorporation in the shell (Tynan et al., *in*
424 *press*; Vander Putten et al., 2000). Given that alternative explanations for Mg/Ca variations
425 are not currently viable, the mean Mg/Ca content in oyster shells can be used to
426 characterize the living sites of specimens of unknown origin. Indeed, Bougeois et al. (2014,
427 2016) tested a variety of models on Eocene oyster shells from the Proto-Paratethys
428 epicontinental sea and the best fitting model for their shells corresponded to a model
429 defined with no direct influence of freshwater. We propose to use such an empirical
430 relationship to identify the environment of collection sites visited by fishermen during
431 Antiquity. The specific use for these models is practical here as the shells used in this study
432 were unearthed from a locality different to that of the (unknown) living environment of the
433 oysters.

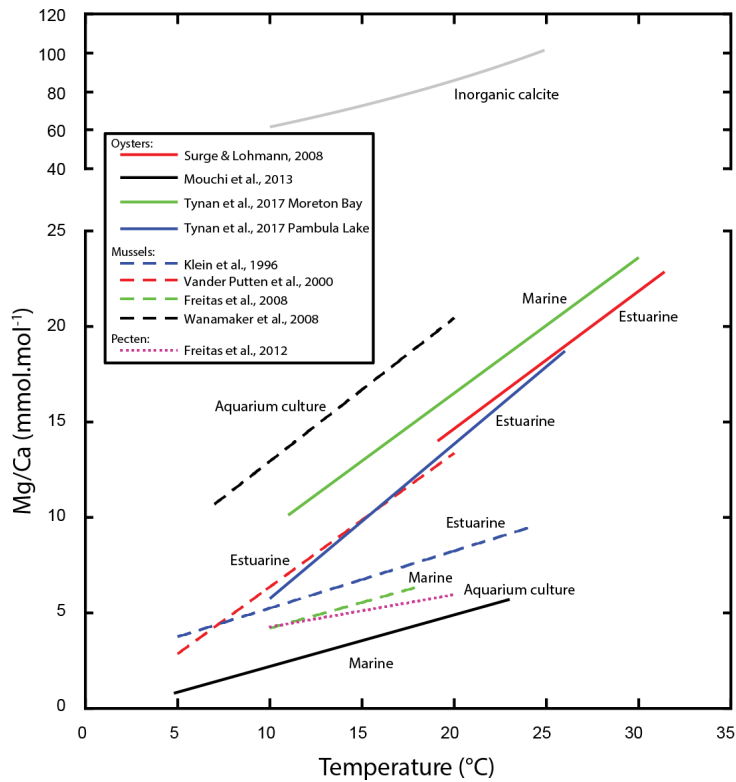
434 A variety of shell Mg/Ca range values have been reported in the literature for normal
435 seawater temperature settings (Fig. 7). The differences transcribed in these relationships
436 probably represent several forcing factors of Mg incorporation.

437 Firstly, contrary to $\delta^{18}\text{O}$ that is in equilibrium with seawater for most molluscs and
438 foraminifera (Epstein et al., 1953; Erez and Luz, 1983), taxonomy has been suggested to have
439 an impact on Mg incorporation (Elderfield et al., 1996) but it appears not to be the case for
440 mussels and oysters, as indicated by the similar relationships (Fig. 7) found by Vander Putten
441 et al. (2000; *M. edulis*), Surge and Lohmann (2008; *C. virginica*) and Tynan et al. (*in press*;
442 *Saccostrea glomerata*). Moreover, similar Mg/Ca ranges were measured from specimens of
443 two oyster species (*O. edulis* and *C. gigas*) bred simultaneously on the same site (Mouchi et
444 al., 2013).

445 Shell Mg/Ca range is similar in the specimens bred in the same location (Mouchi et al., 2013;
446 Surge and Lohmann, 2008; Vander Putter et al., 2000; Tynan et al., *in press*), indicating that
447 the range of incorporation of Mg in bivalve shells depends much more on the locality and
448 the type of hydrologic settings than on potential vital effects. Indeed, shells from all
449 estuarine locations exhibit a strong Mg incorporation (Klein et al., 1996; Surge and Lohmann,
450 2008; Tynan et al., *in press*; Vander Putter et al., 2000), while all but one marine location
451 from those studied correspond to a weak Mg incorporation in bivalve shells. The location
452 that do not fit this observed relationship, Moreton Bay (Tynan et al., *in press*), presents a
453 typical marine salinity (35.1-36.7 ‰) but corresponds to a sheltered area with a relatively
454 long residence time of seawater (up to 100 days). This may be responsible for the
455 differences observed in Mg incorporation in bivalve shells compared to other sites with
456 more open marine influence.

457 The equation derived by Wanamaker et al. (2008) for *M. edulis* indicates high values of shell
458 Mg/Ca compared to other studies for similar temperatures. This model was established from
459 a laboratory experiment using water derived from seawater collected in the Damariscotta
460 River, Maine, far from the open sea. At this location, salinity is known to fluctuate from
461 season to season between 5 to 28 ‰ (Thompson et al., 2006), suggesting strong freshwater
462 input from rivers. The *M. edulis* models providing equivalent temperature values were
463 defined from locations presenting both open marine influence and freshwater input (Klein et
464 al., 1996; Freitas et al., 2008).

465



466

467 Figure 7: Bivalve shell Mg/Ca range values for common seawater temperature settings from
 468 various published studies. Each relationship has been established from a different locality.
 469 Solid lines correspond to relationships measured from oysters, dashed lines correspond to
 470 the *Mytilus* mussel genus and the dotted line corresponds to *Pecten maximus*. Relationship
 471 for inorganic calcite is given for comparison.

472

473 The six specimens from our study can be associated with the environmental relationships of
 474 these models and by extension to the type of settings according to their Mg/Ca range values.
 475 In particular, specimens US547-1, US654-1 and US654-3 probably lived at locations subject
 476 to both marine and freshwater influence (Mg/Ca range: approx. 3-12 mmol.mol⁻¹).

477 Interestingly, the age model from CL fluctuations indicates that the higher Mg/Ca values in
 478 specimen US654-1 occur during the winter months and the lower values during the summer
 479 months, as confirmed by temperatures calculated from $\delta^{18}\text{O}$ from this specimen. Such an

480 relationship between seasonal growth / temperature and Mn incorporation indicates that
481 Mn (as a CL activator) in this specimen is seasonally opposed to that of the other specimens
482 from this study and all modern specimens studied by Lartaud et al. (2010c) and Mouchi et al.
483 (2013). Such a difference may be caused by differences in seawater chemistry between the
484 living locality of US654-1 when compared to localities with no important freshwater input.
485 Additional examination under CL of other modern oyster shells from confirmed estuarine
486 areas would be required to check this assumption. Therefore, the locations of origin of
487 specimens US547-1, US654-1 and US654-3 may correspond to lagoons with partial
488 freshwater input from small rivers or groundwater.

489 Specimens US118-3 and US915-1, with low Mg/Ca values (approx. 0-5 mmol.mol⁻¹), are
490 generally compatible with an open marine environment. Specimen US118-3 presents the
491 particularity to change the amplitude of Mg/Ca values from simple to double around 5 mm
492 from the start of the umbo (after the second year of growth, according to the CL seasonal
493 calibration). This can be interpreted as a change in local hydrologic regime during the
494 organism lifespan, corresponding to an increased freshwater input. Growth rates (based on
495 CL seasonal calibration; Fig. 2) are indeed different for this specimen compared to the
496 others, as the shell appears to have grown faster during its fourth and seventh year and
497 slower the other years, suggesting an instable site in terms of food supply and favourable
498 environmental factors.

499 Finally, the Mg/Ca range in specimen US46-2 (approx. 10-30 mmol.mol⁻¹) indicates a strong
500 freshwater influence. As $\delta^{18}\text{O}$ values also reflect strong impact of freshwater input, the living
501 locality of this specimen must have been close to a river outlet.

502 The French Mediterranean coastline comprises numerous lagoons (Derolez et al., 2015) that
503 are partly supplied by freshwater from rivers and karstic groundwaters (Fleury et al., 2007).

504 Groundwater can have a strong influence on the water composition of lagoons and
505 substantially change water chemistry compared to adjacent areas (Stieglitz et al., 2013).
506 Therefore, the heterogeneity of geochemical signals in the oyster shells presented here
507 reflects a diversity of locality settings, most likely on the Mediterranean coastline.
508 The precise identification of the localities from which originated the oysters is impossible
509 with the present data and would require substantial analyses of the geochemistry of
510 multiple oyster shells from a variety of areas on the French Mediterranean coastline to be
511 compared with that of these specimens (although it cannot currently be excluded that these
512 specimens originated from other regions than the Mediterranean coastline). However, it
513 appears clear that specimen US46-2 originated from a different type of environment than
514 the other specimens. The locality for this specimen was subjected to an alternating and
515 strong freshwater influence, as suggested by the $\delta^{13}\text{C}$ and $\delta^{18}\text{O}$ data (Fig. 5). The largest
516 freshwater source in this region of the Mediterranean is the Rhone River. The Rhone River
517 forms a delta, hence providing an important flow of freshwater and large floods which could
518 possibly correspond to the results of $\delta^{18}\text{O}$ and mean Mg/Ca from this specimen.
519 However, the Rhone River may not have been the origin of specimen US46-2 as this outlet
520 (whose limits strongly varied over the ages) is too dynamic and unstable to grant survival of
521 long term oyster communities. Specimen US46-2 may have been collected from a large
522 estuary, close to the river outlet. An exact location for oyster harvest is however impossible
523 to determine at this time, partly due to the current complex coastline with multiple lagoons,
524 and partly because the position of the shoreline has changed since Antiquity (Bardot-Cambot
525 and Forest, 2015; Rey et al., 2005) and most lagoons are nowadays entirely emerged.

526 **Conclusion**

527 This study used two geochemical proxies for environmental reconstruction and

528 cathodoluminescence from six oyster shells on archaeological specimens dated from the 3rd
529 century AD to the 5th century AD and found in archaeological sites in Lyon, Central France.
530 Though the original living locality of these specimens is not known, the geochemical
531 heterogeneity among the shells indicates that these specimens did not live in the same area
532 and were under the influence of different mixing waters. Stable isotope analyses from three
533 shells indicate various regimes in freshwater input, with one specimen probably originating
534 from a locality in direct proximity to a river outlet while the two others present more stable
535 marine conditions.

536 As Mg/Ca ratio amplitude in bivalve shells has been reported to be different according to the
537 locality and the hydrologic setting in equivalent temperature ranges, we suggest that the
538 geochemical differences observed in each shell can be used to identify the environment
539 (estuary, lagoon, marine) from which the specimens originated. Our results indicate that
540 fishermen were probably not restricted to a single locality for oyster collection during
541 Antiquity but harvested oysters from a variety of areas. This study also highlights the
542 importance of careful choice of a Mg/Ca model to estimate palaeotemperatures in coastal
543 areas where freshwater input may have been a factor.

544

545 **Acknowledgements**

546 The authors would like to thank Nathalie Labourdette from UPMC for analyzing the isotope
547 samples. We are grateful to Elise Dufour for giving us access to the micromill at the MNHN.

548 We also thank Quentin Crowley for the editing he provided to this manuscript. Finally, we
549 would like to thank Michel Fialin and Nicolas Rividi from the Camparis service for their help
550 and time during the EPMA experiments.

551

552 **References**

- 553 Anderson, T.F., Arthur, M.A., 1983. Stable isotopes of oxygen and carbon and their
554 application to sedimentologic and paleoenvironmental problems. *In*: Arthur, M.A., Anderson,
555 T.F., Kaplan, I.R., Veizer, J., Land, L. (Eds.), *Stable isotopes in sedimentary geology*, S.E.P.M.,
556 Short Course, 1-151.
- 557 Bardot-Cambot, A., 2014. Consommer dans les campagnes de la Gaule Romaine. *Revue du*
558 *Nord*, Hors-série, Collection Art et Archéologie, 21, 109-123.
- 559 Bardot-Cambot, A., Forest, V., 2013. Ostréiculture et mytiliculture à l'époque romaine ? Des
560 définitions modernes à l'épreuve de l'archéologie. *Revue archéologique*, 2013 fascicule 2,
561 367-388.
- 562 Bardot-Cambot, A., Forest, V., 2015. Du conchylioreste à l'environnement : de la nature à
563 l'homme, de l'homme à la nature. *In*: Bardot-Cambot, A., Trannoy, L. (Eds.), *L'environnement*
564 *en mémoire*, Presses universitaires de Rennes, ISBN 978-2-7535-4050-7, 11-24.
- 565 Bertrand, E., 2011. 16, rue Bourgelat – 69002 Lyon. Institut Saint-Vincent-de-Paul. Rapport
566 de fouille d'archéologie préventive, Service archéologique de la ville de Lyon, 508 p.
- 567 Bougeois, L., de Rafélis, M., Reichart, G.-J., de Nooijer, L.J., Nicollin, F., Dupond-Nivet, G.,
568 2014. A high resolution study of trace elements and stable isotopes in oyster shells to
569 estimate Central Asian Middle Eocene seasonality. *Chemical Geology*, 363, 200-212.
- 570 Bougeois, L., de Rafélis, M., Reichart, G.-J., de Nooijer, L.J., Dupond-Nivet, G., 2016. Mg/Ca in
571 fossil oyster shells as palaeotemperature proxy, an example from the Palaeogene of Central
572 Asia. *Palaeogeography, Palaeoclimatology, Palaeoecology*, 441, 611-626.
- 573 Carozza, J.-M., Puig, C., Valette, P., Odier, T., 2010. La plaine du Roussillon au cours de
574 l'Holocène : apport d'une démarche géoarchéologique et géomorphologique à la
575 connaissance des interactions homme-milieu. *Archéologie des rivages méditerranéens : 50*

576 *ans de recherche*, Errance, 37-46.

577 Carré, M., Bentaleb, I., Bruguier, O., Ordinola, E., Barrett, N.T., Fontugne, M., 2006.

578 Calcification rate influence on trace element concentrations in aragonitic bivalve shells:
579 evidences and mechanisms. *Geochimica et Cosmochimica Acta*, 70, 19, 4906–4920.

580 Craig, H., 1965. Measurements of oxygen isotope paleotemperatures. *In*: Tongiorgi, E. (Ed.),
581 Stable Isotopes in Oceanographic Studies and Paleotemperatures, Consiglio Nazionale Delle
582 Ricerche Laboratorio Di Geologia Nucleare, 161-182.

583 de Rafélis, M., Renard, M., Emmanuel, L., Durlet, C., 2000. Apport de la
584 cathodoluminescence à la connaissance de la spéciation du manganèse dans les carbonates
585 pélagiques. *Comptes Rendus de l'Académie des Sciences - Series IIA - Earth and Planetary
586 Science*, 330, 391-398.

587 Derolez, V., Oheix, J., Ouisse, V., Munaron, D., Fiandrino, A., Messiaen, G., Hubert, C.,
588 Lamoureux, A., Malet, N., Fortune, M., Berard, L., Mortreux, S., Guillou, J.-L., 2015. Suivi
589 estival des lagunes méditerranéennes françaises - Bilan des résultats 2014. IFREMER
590 publication <http://archimer.ifremer.fr/doc/00273/38461/>.

591 Dubar, M., 2003. The Holocene deltas of Eastern Provence and the French Riviera:
592 geomorphological inheritance, genesis and vulnerability. *Geomorphologie : relief, processus,
593 environnement*, 4, 263-270.

594 Duprey, N., Lazareth, C.E., Dupouy, C., Butscher, J., Farman, R., Maes, C., Cabioch, G., 2015.

595 Calibration of seawater temperature and $\delta^{18}\text{O}$ seawater signals in *Tridacna maxima*'s
596 $\delta^{18}\text{O}$ shell record based on in situ data. *Coral Reefs*, 34, 437-450.

597 Elderfield, H., Bertram, C.J., Erez, J., 1996. A biomineralization model for the incorporation of
598 trace elements into foraminiferal calcium carbonate. *Earth and Planetary Science Letters*,
599 142, 409-423.

600 Emery, K.A., Wilkinson, G.M., Camacho-Ibar, V.F., Pace, M.L., McGlathery, K.J., Sandoval-Gil,
601 J.M., Hernandez-Lopez, J., 2016. Resource use of an aquacultured oyster (*Crassostrea gigas*)
602 in the reverse estuary Bahia San Quintin, Baja California, Mexico. *Estuaries and Coasts*, 39,
603 866-874.

604 Epstein, S., Mayeda, T., 1953. Variation of O¹⁸ content of waters from natural sources.
605 *Geochimica et Cosmochimica Acta*, 4, 213-224.

606 Epstein, S., Buchsbaum, R., Lowenstam, H.A., Urey, H.C., 1951. Carbonate-water isotopic
607 temperature scale. *Bulletin of the Geological Society of America*, 62, 417-426.

608 Epstein, S., Buchsbaum, R., Lowenstam, H.A., Urey, H.C., 1953. Revised carbonate-water
609 isotopic temperature scale. *Bulletin of the Geological Society of America*, 64, 1315-1326.

610 Erez, J., Luz, B., 1983. Experimental paleotemperature equation for planktonic foraminifera.
611 *Geochimica et Cosmochimica Acta*, 47, 1025-1031.

612 Faget D., 2007. Cultiver la mer : biodiversité marine et développement de l'ostréiculture
613 dans le Midi méditerranéen français au XIXe siècle. *In: Annales du Midi : revue*
614 *archéologique, historique et philologique de la France méridionale*, Tome 119, 258. Les
615 triens mérovingiens en Limousin, 207-226, doi : 10.3406/anami.2007.7177.

616 Fleury, P., Bakalowicz, M., de Marsily, G., 2007. Submarine springs and coastal karst aquifers:
617 A review. *Journal of Hydrology*, 339, 79-92.

618 Freitas, P., Clarke, L., Kennedy, H., Richardson, C., 2008. Inter-and intra-specimen variability
619 masks reliable temperature control on shell Mg/Ca ratios in laboratory and field cultured
620 *Mytilus edulis* and *Pecten maximus* (Bivalvia). *Biogeoscience Discussions*, 5.

621 Freitas, P.S., Clarke, L.J., Kennedy, H., Richardson, C.A., 2012. The potential of combined
622 Mg/Ca and $\delta^{18}\text{O}$ measurements within the shell of the bivalve *Pecten maximus* to estimate
623 seawater $\delta^{18}\text{O}$ composition. *Chemical Geology*, 291, 286-293.

624 Gaudron, S.M., Grangeré, K., Lefebvre, S., 2016. The comparison of $\delta^{13}\text{C}$ values of a deposit-
625 and a suspension-feeder bio-indicates benthic vs. pelagic couplings and trophic status in
626 contrasted coastal ecosystems. *Estuaries and Coasts*, 39, 731-741.

627 Gillikin, D.P., Lorrain, A., Navez, J., Taylor, J.W., André, L., Keppens, E., Baeyens, W., Dehairs,
628 F., 2005. Strong biological controls on Sr /Ca ratios in aragonitic marine bivalve shells.
629 *Geochemistry, Geophysics, Geosystems*, 6, 5, doi:10.1029/2004GC000874.

630 Hofmann, E., in prep. Fouille de l'îlot central de l'Antiquaille (Lyon, 5e arrondissement).
631 Rapport de fouilles.

632 Kirby, M.X., Soniat, T.M., Spero, H.J., 1998. Stable isotope sclerochronology of Pleistocene
633 and Recent oyster shells (*Crassostrea virginica*). *Palaios*, 13, 560-569.

634 Klein, R.T., Lohmann, K.C., Thayer, C.W., 1996. Bivalve skeletons record seas-surface
635 temperature and $\delta^{18}\text{O}$ via Mg/Ca and $^{18}\text{O}/^{16}\text{O}$ ratios. *Geology*, 24, 415-418.

636 Langlet, D., Alunno-Bruscia, M., de Rafélis, M., Renard, M., Roux, M., Schein, E., Buestel, D.,
637 2006. Experimental and natural cathodoluminescence in the shell of *Crassostrea gigas* from
638 Thau lagoon (France): ecological and environmental implications. *Marine Ecology Progress*
639 *Series*, 317, 143-156.

640 Lartaud, F., 2007. Les fluctuations haute fréquence de l'environnement au cours des temps
641 géologiques. Mise au point d'un modèle de référence actuel sur l'enregistrement des
642 contrastes saisonniers dans l'Atlantique nord. Ph.D thesis, UPMC-Paris 06, 336 p.

643 Lartaud, F., Langlet, D., de Rafélis, M., Emmanuel, L., Renard, M., 2006. Description of
644 seasonal rythmicity in fossil oyster shells *Crassostrea aginensis* Tournouer, 1917 (Aquitanian)
645 and *Ostrea bellovacina* Lamarck, 1806 (Thanetian). Cathodoluminescence and
646 sclerochronological approaches. *Geobios*, 39, 845-852. doi:10.1016/j.geobios.2005.11.001.

647 Lartaud, F., Emmanuel, L., de Rafélis, M., Ropert, M., Labourdette, N., Richardson, C.A.,

648 Renard, M., 2010a. A latitudinal gradient of seasonal temperature variation recorded in
649 oyster shells from the coastal waters of France and The Netherlands. *Facies*, 56, 13-25.

650 Lartaud, F., Emmanuel, L., De Rafelis, M., Pouvreau, S., Renard, M., 2010b. Influence of food
651 supply on the $\delta^{13}\text{C}$ signature of mollusc shells: implications for palaeoenvironmental
652 reconstitutions. *Geo-Marine Letters*, 30, 23-34.

653 Lartaud, F., de Rafélis, M., Ropert, M., Emmanuel, L., Geairon, P., Renard, M., 2010c. Mn
654 labelling of living oysters: Artificial and natural cathodoluminescence analyses as a tool for
655 age and growth rate determination of *C. gigas* (Thunberg, 1793) shells. *Aquaculture*, 300,
656 206-217.

657 Lazareth, C.E., Vander Putten, E., André, L., Dehairs, F., 2003. High-resolution trace element
658 profiles in shells of the mangrove bivalve *Isognomon ehippium*: a record of environmental
659 spatio-temporal variations? *Estuarine, Coastal and Shelf Science*, 57, 1103-1114.

660 Lorrain, A., Gillikin, D., Paulet, Y.-M., Chauvaud, L., Le Mercier, A., Navez, J., André, L., 2005.
661 Strong kinetic effects on Sr/Ca ratios in the calcitic bivalve *Pecten maximus*. *Geology*, 33, 12,
662 965-968.

663 Luterbacher, J., Werner, J.-P., Smerdon, J.-E., Fernandez-Donado, L., Gonzales-Rouco, J.-F.,
664 Barriopedro, D., Ljungqvist, F.-C., Buntgen, U., Zorita, E., 2016. European summer
665 temperatures since Roman Times. *Environmental Research Letters*, 11, 024001.

666 McCrea, J.M., 1950. On the isotopic chemistry of carbonates and a paleotemperature scale.
667 *The Journal of Chemical Physics*, 18, 849-857.

668 McConnaughey, T.A., Gillikin, D.P., 2008. Carbon isotopes in mollusk shell carbonates. *Geo-*
669 *Marine Letters*, 28, 287-299. doi: 10.1007/s00367-008-0116-4.

670 Mouchi, V., de Rafélis, M., Lartaud, F., Fialin, M., Verrecchia, E., 2013. Chemical labelling of
671 oyster shells used for time-calibrated high-resolution Mg/Ca ratios: A tool for estimation of

672 past seasonal temperature variations. *Palaeogeography, Palaeoclimatology, Palaeoecology*,
673 373, 66-74.

674 Pierre, C., 1999. The oxygen and carbon isotope distribution in the Mediterranean water
675 masses. *Marine Geology*, 153, 41-55.

676 Poulain, C., Gillikin, D.P., Thébault, J., Munaron, J.M., Bohn, M., Robert, R., Paulet, Y.-M.,
677 Lorrain, A., 2015. An evaluation of Mg/Ca, Sr/Ca, and Ba/Ca ratios as environmental proxies
678 in aragonite bivalve shells. *Chemical Geology*, 396, 42-50.

679 Prendergast, A.L., Azzopardi, M., O'Connell, T.C., Hunt, C., Barker, G., Stevens, R.E., 2013.
680 Oxygen isotopes from *Phorcus (Osilinus) turbinatus* shells as a proxy for sea surface
681 temperature in the central Mediterranean: A case study from Malta. *Chemical Geology*, 345,
682 77-86.

683 Raynal, O., Bouchette, F., Certain, R., Séranne, M., Sabatier, P., Lofi, J., Dezileau, L., Briquieu,
684 L., Pezard, P., Courp, P., 2010. Holocene evolution of languedocian lagoonal environment
685 controlled by inherited coastal morphology (northern Gulf of Lions, France). *Bulletin de la*
686 *Société Géologique de France*, 181, 2, 211-224.

687 Rescanières, S., 2002. Essai sur le cadre géographique antique du Narbonnais. *In* : Dellong E.
688 (Ed.), Narbonne et le Narbonnais (11/1), Carte archéologique de la Gaule, Paris, France, 44-
689 51.

690 Rey, T., Lefevre, D., Vella, C., 2005. Données nouvelles sur les lobes deltaïques du paléogolf
691 d'Aigues-Mortes à l'Holocène [Petite Camargue, France]. *Quaternaire*, 16, 329-338.

692 Rey, T., Lefevre, D., Vella C., 2009. Deltaic plain development and environmental changes in
693 the Petite Camargue, Rhône Delta, France, in the past 2000 years. *Quaternary Research*, 71,
694 284-294.

695 Richardson, C., Collis, S., Ekaratne, K., Dare, P., Key, D., 1993. The age determination and

696 growth rate of the European flat oyster, *Ostrea edulis*, in British waters determined from
697 acetate peels of umbo growth lines. *ICES Journal of Marine Science*, 50, 493-500.

698 Rohling, E.J., 2000. Paleosalinity: confidence limits and future applications. *Marine Geology*,
699 163, 1-11.

700 Saenger, C., Wang, Z., 2014. Magnesium isotope fractionation in biogenic and abiogenic
701 carbonates: implications for paleoenvironmental proxies. *Quaternary Science Reviews*, 90,
702 1-21.

703 Schöne, B.R., Gillikin, D.P., 2013. Unraveling environmental histories from skeletal diaries —
704 Advances in sclerochronology. *Palaeogeography, Palaeoclimatology, Palaeoecology*, 373, 1-
705 5.

706 Stenzel, H.B., 1971. Oysters. *Treatise on Invertebrate Paleontology*, 3, 953-1184.

707 Stieglitz, T., van Beek, P., Souhaut, M., Cook, P.G., 2013. Karstic groundwater discharge and
708 seawater recirculation through sediments in shallow coastal Mediterranean lagoons,
709 determined from water, salt and radon budgets. *Marine Chemistry*, 156, 73-84.

710 Sunda, W.G., Huntsman, S.A., 1985. Regulation of cellular manganese and manganese
711 transport rates in the unicellular alga *Chlamydomonas*. *Limnology and Oceanography*, 30,
712 567-586.

713 Surge, D., Walker, K.J., 2006. Geochemical variation in microstructural shell layers of the
714 southern quahog (*Mercenaria campechiensis*): Implications for reconstructing seasonality.
715 *Palaeogeography, Palaeoclimatology, Palaeoecology*, 237, 182-190.

716 Surge, D., Lohmann, K.-C., 2008. Evaluating Mg/Ca ratios as a temperature proxy in the
717 estuarine oyster, *Crassostrea virginica*. *Journal of Geophysical Research*, 113, G02001.

718 Surge, D.M., Lohmann, K.C., Dettman, D. L., 2001. Controls on isotopic chemistry of the
719 American oyster, *Crassostrea virginica*: Implications for growth patterns. *Palaeogeography*,

720 *Palaeoclimatology, Palaeoecology*, 172, 283-296.

721 Surge, D., Lohmann, K.C., Goodfriend, G.A., 2003. Reconstructing estuarine conditions:
722 Oyster shells as recorders of environmental change, southwest Florida. *Estuarine, Coastal*
723 *and Shelf Science*, 57, 737-756.

724 Thompson, B., Perry, M.J., Davis, C., 2006. Phytoplankton in the Damariscotta River Estuary.
725 *Marine Research in focus*, Sept. 2006, 3, 4 p.

726 Tynan, S., Opdyke, B.N., Walczak, M., Eggins, S., Dutton, A., in press. Assessment of Mg/Ca in
727 *Saccostrea glomerata* (the Sydney rock oyster) shell as a potential temperature record.
728 *Palaeogeography, Palaeoclimatology, Palaeoecology*,
729 <http://dx.doi.org/10.1016/j.palaeo.2016.08.009>.

730 Ullmann, C.V., Böhm, F., Rickaby, R.E.M., Wiechert, U., Korte, C., 2013. The Giant Pacific
731 Oyster (*Crassostrea gigas*) as a modern analog for fossil ostreoids: Isotopic (Ca, O, C) and
732 elemental (Mg/Ca, Sr/Ca, Mn/Ca) proxies. *Geochemistry, Geophysics, Geosystems*, 14, 4109-
733 4120, doi:10.1002/ggge.20257.

734 Urey, H.C., Lowenstam, H.A., Epstein, S., McKinney, C.R., 1951. Measurement of
735 paleotemperatures and temperatures of the Upper Cretaceous of England, Denmark, and
736 the Southeastern United States. *Bulletin of the Geological Society of America*, 62, 399-416.

737 Vander Putten, E., Dehairs, F., Keppens, E., Baeyens, W., 2000. High resolution distribution of
738 trace elements in the calcite shell layer of modern *Mytilus edulis*: environmental and
739 biological controls. *Geochimica et Cosmochimica Acta*, 64, 997-1011.

740 Voelker, A.H.L., Colman, A., Olack, G., Waniek, J.J., Hodell, D., 2015. Oxygen and hydrogen
741 isotope signatures of Northeast Atlantic water masses. *Deep-Sea Research II*, 116, 89-106.

742 Wanamaker, A.D., Kreutz, K.J., Wilson, T., Borns Jr., H.W., Introne, D.S., Feindel, S., 2008.
743 Experimentally determined Mg/Ca and Sr/Ca ratios in juvenile bivalve calcite for *Mytilus*

744 *edulis*: implications for paleotemperature reconstructions. *Geo-Marine Letters*, 28, 359-368.

745 Walther, B.D., Rowley, J.L., 2013. Drought and flood signals in subtropical estuaries recorded

746 by stable isotope ratios in bivalve shells. *Estuarine, Coastal and Shelf Science*, 133, 235-243.

747

748 SUPPLEMENTARY INFORMATION

749

750 Table 1: Thermodependance equations of Mg/Ca in mollusc shells from breeding experiments
 751 according to the type of locality.

752

ENVIRONMENT	SPECIES	EQUATION	REFERENCE
ESTUARINE	<i>Crassostrea virginica</i>	$Mg/Ca = 0.72 * T + 0.25$	Surge and Lohmann (2008)
	<i>Mytilus edulis</i>	$Mg/Ca = 0.70 * T - 0.63$	Vander Putten et al. (2000)
	<i>Mytilus trossulus</i>	$Mg/Ca = 0.30 * T + 2.25$	Klein et al. (1996)
	<i>Saccostrea glomerata</i>	$Mg/Ca = 0.81 * T - 2.35$	Tynan et al. (2016)
OPEN MARINE	<i>Crassostrea gigas</i>	$Mg/Ca = 0.27 * T - 0.5$	Mouchi et al. (2013)
	<i>Mytilus edulis</i>	$Mg/Ca = 0.27 * T + 1.5$	Freitas et al. (2008)
	<i>Saccostrea glomerata</i>	$Mg/Ca = 0.71 * T + 2.31$	Tynan et al. (2016)
AQUARIUM	<i>Mytilus edulis</i>	$Mg/Ca = 0.75 * T + 5.44$	Wanamaker et al. (2008)
	<i>Pecten maximus</i>	$Mg/Ca = 0.17 * T + 2.56$	Freitas et al. (2012)

753